Electron distributions in kinetic scale field line resonances: A comparison of simulations and observations

P.A. Damiano[1,2], C.C. Chaston[3], A.J. Hull[3], and J.R. Johnson[4]

Peter Damiano, padamiano@alaska.edu

[1]Geophysical Institute, University of Alaska Fairbanks, Fairbanks, AK 99775

[2]Princeton Plasma Physics Laboratory, Princeton University, Princeton, NJ 08543

[3]Space Sciences Laboratory, University of California, Berkeley, CA 94720

[4]Department of Engineering and Computer Science, Andrews University, Berrien Springs, Michigan

This article has been accepted for publication and undergone full peer review but has not been through the copyediting, typesetting, pagination and proofreading process, which may lead to differences between this version and the Version of Record. Please cite this article as doi: 10.1029/2018GL077748

Observations in kinetic scale field-line resonances, or eigenmodes of the geomagnetic field, reveal highly field-aligned plateaued electron distributions. By combining observations from the Van Allen Probes and Cluster spacecraft with a hybrid kinetic gyro-fluid simulation we show how these distributions arise from the non-local self-consistent interaction of electrons with the wave field. This interaction is manifest as electron trapping in the standing wave potential. The process operates along most of the field-line and qualitatively accounts for electron observations near the equatorial plane and at higher latitudes. In conjunction with the highly field-aligned plateaus, loss cone features are also evident which result from the action of the upward directed wave parallel electric field on the un-trapped electron populations.

Keypoints:

- Electron distributions in kinetic field-line resonances exhibit highly field-aligned plateaued cores due to electron trapping.
- Loss cone features result from the precipitation of higher energy un-trapped electrons.
- These electron distribution features are evident in both simulations and observations

1. Introduction

Field line resonances, or standing shear Alfvén waves along the Earth's closed magnetic field lines, are an important mechanism for coupling the magnetosphere and ionosphere leading to the formation of some auroral arcs [e.g. *Xu et al.*, 1993; *Samson et al.*, 2003; *Lotko et al.*, 1998]. They have been noted in observations for decades, both in the auroral zone [*Samson et al.*, 2003; *Lotko et al.*, 1998] and inner magnetosphere (where they play a role in the radial diffusion of electrons [e.g. *Elkington*, 2006; *Hudson et al.*, 2008; *Li et al.*, 2016]) and have been studied extensively with MHD simulations [e.g. *Rankin et al.*, 1993; *Rankin et al.*, 1994; *Rickard and Wright*, 1994; *Voronkov et al.*, 1997; *Claudepierre et al.*, 2010; *Claudepierre et al.*, 2016]. The interaction between the bulk electron population and these waves has also been the subject of more recent studies using kinetic simulation methods [e.g. *Damiano et al.*, 2003; *Damiano et al.*, 2007; *Rankin et al.*, 2007; *Damiano and Johnson*, 2012].

While extensive, the majority of this past simulation work has been performed at large perpendicular scale lengths with consideration of the role of kinetic scale lengths on the evolution of these waves [*Wei et al.*, 1994; *Streltsov and Lotko*, 1995, 1997; *Streltsov et al.*, 1998] and the electron dynamics within them [*Damiano et al.*, 2003; *Damiano et al.*, 2005; *Rankin et al.*, 2007]. The importance of these kinetic scale lengths has recently been reinforced by the observations of *Chaston et al.* [2014, 2015], which illustrated the existence of field line resonances on ion gyroradius scale lengths in the inner magnetosphere. From the point of view of the electron dynamics, waves on these kinetic scale lengths are important as they result in the radial diffusion of electrons via drift-bounce resonance [*Chaston et al.*,

2017] and contribute to electron energization via parallel electric fields. This energization however, should be different in character to that which is presented at larger perpendicular scale lengths, where mirror force effects are likely to be the primary contributor to the generation of $E_{||}$ [e.g. *Nakamura*, 2000; *Damiano and Wright*, 2008; *Damiano and Johnson*, 2012].

In this work we use a 2D hybrid gyrofluid-kinetic electron (GKE) model to examine the interaction of electrons with these kinetic scale field line resonances and compare the results with observations of separate events from the Van Allen probes and Cluster spacecraft. The Van Allen Probes observations are centered close to the equatorial plane and the Cluster observations are at higher latitudes. While not conjunctive, this latitudinal separation allows a general examination of how kinetic scale field line resonances (KFLRs) and the supporting electron distributions vary along the nearly dipolar geomagnetic field, where the observations are recorded. Additionally, the particle detectors on the Cluster spacecraft allow for a higher temporal cadence (4 seconds) than does those on Van Allen Probes (11 seconds), which allows us to investigate features that may not be resolved from the Van Allen Probes. The remainder of the paper is broken up into 3 sections. Section 2 presents an overview of the observations considered. Section 3 presents simulations results while Section 4 summarizes our conclusions.

2. Observations

2.1. Van Allen probes observations

Figure 1 presents observations of an interval of low frequency electromagnetic wave activity recorded during the main phase of a geomagnetic storm reported by *Chaston*

et al. [2015]. The spacecraft at this time was located at $L = 6$ with a magnetic latitude of $\sim 18^o$. The largest amplitudes are observed over the sub-interval indicated on Figure 1a that is centered on 0551:30 UT and coincident with the appearance of enhanced energetic electron fluxes. The fields measurements over this sub-interval are shown in Figures 1b and 1c. Cross spectral analyses of these fields time series revealed that the field variations are composed of a mix of traveling waves and field-line eigenmodes with transverse scales of the order of the bulk ion gyro-radii - i.e. KFLRs. Examination of the electron distributions shown in Figures 1d and 1e in these waves over the intervals shaded mauve in Figures 1b and 1c reveals a broad-plateau in phase space density composed of field-aligned electrons counter-streaming along the geomagnetic field. Electron distributions with similar form are invariably embedded within the wavefields of dispersive Alfvén waves in a broad range of magnetospheric environments [*Chaston et al.*, 1999; *Wygant et al.*, 2002; *Damiano et al.*, 2016]. Simulations have illustrated that such distributions can be formed under the influence of traveling kinetic Alfvén wave pulses [*Damiano et al.*, 2016] or wave packets [*Watt and Rankin*, 2009], but the Van Allen probes observations suggest a distribution of both traveling and standing modes. How the standing modes contribute to the observed features of the electron distribution remains an open question.

2.2. Cluster observations

In order to compare features of electron distributions and currents associated with dispersive scale field-line resonances at lower altitudes we examined the substorm event reported by *Hull et al.* [2016]. In that study, the Cluster fleet was at an altitude of 3.4 R_E in the upper edge of the auroral acceleration region, when standing dispersive Alfvén modes

were observed to form during the onset/early expansion phase of a poleward boundary intensification triggered substorm. At this time, the Cluster spacecraft were located at a magnetic latitude of 31^o and L-shell 6.7. The standing modes formed in conjunction with the injection of a hotter denser magnetospheric plasma in a large scale upward current region initially characterized to have predominently travelling Alfvén wave characteristics over the same frequency range [*Hull et al.*, 2016]. Data from one of the Cluster spacecraft (SC4) is summarized in Figure 2. Vertical regions shaded in mauve delineate an area of interest, where dispersive scale FLR signatures are observed. The quasi-periodic standing nature of the system is clearly discernible from the parallel current signatures (Figures 2c and 2f), which are shown to alternate between instances of upward (red) and downward (green) current. Figures 2g - 2i show electron distributions at the times indicated by the mauve shaded intervals in Figures 2d - 2f. Two of the distributions (Figures 2g and 2i) are from local upward current regions, while one (Figure 2h) is from a localized downward current region. The distributions are generally composed of two components: a hot plasma sheet component, and a lower energy field-aligned core component. Unlike the nearly symmetric distributions from Van Allen Probes, these distributions have asymmetric features that vary in concert with the sense of the current. Particularly, the skew of the core electrons is oriented opposite to the sign of the parallel current. Loss-cone features in the field-opposed direction are also apparent in the upward current distributions (see Figures 2g and 2i).

3. Simulations

In order to investigate the evolution of the electron distributions under the influence of the kinetic scale field line resonances, we simulate the system using the 2-D Gyro-fluid Kinetic Electron (GKE) model [*Damiano et al.*, 2007; *Damiano et al.*, 2015], which was recently used to study the case of traveling kinetic Alfvén wave pulses [*Damiano et al.*, 2015; *Damiano et al.*, 2016]. The model (which is the gyrofluid extension of the hybrid MHD-kinetic electron model [*Damiano et al.*, 2007]) has also previously been used to study large perpendicular scale field line resonances in the auroral zone [*Damiano and Wright*, 2008; *Damiano and Johnson*, 2012]. It treats electron motion along the field line as drift-kinetic and ions with a kinetic-fluid closure [*Damiano et al.*, 2015] based on *Cheng and Johnson* [1999], which includes ion Larmor radius corrections and the physics of the ion polarization current. The dipolar geometry is illustrated in Figure 3a and explicitly includes the field aligned direction (x_1) and the direction across L shells (x_2). The system is independent of the azimuthal coordinate so that $\partial/\partial x_3 = 0$. Thus, although there is azimuthal variation evident in the observations, we are restricted to consideration of purely toroidal modes at present. For the electron energy range considered, this omission will alter the results we describe in detail only.

As with *Damiano et al.* [2007] and *Damiano and Wright* [2008], the system is initialized using an eigenmode solution of the perpendicular electric field for a standing shear Alfvén wave along the dipolar magnetic field line (derived from the model of *Taylor and Walker* [1984]). The perpendicular and parallel profiles of the initial perturbation are displayed in Figures 3b and 3c respectively. To approximately correspond to the considered data

sets (our aim is to stress average or typical conditions), the perturbation is centered on an $L = 6$ field line with a constant density of $n = 1\ cm^{-3}$ and we assume electron and ion temperatures of 1 and 10 keV respectively. In Figure 3b, we assume a perpendicular scale length of 0.1 R_E, which results in a value of $k_\perp \rho_i \sim 1$ in the equatorial plane, given the ion temperature. To allow for a mixture of ions similar to those seen in observations [e.g. *Denton et al.*, 2005], we adjusted the ion mass (allowing for 94% H^+ and 6% O^+) to be 1.95 m_p.

Because the simulation model requires symmetry between the northern and southern hemispheres, we focus on odd numbered nodes and present results for an $n = 5$ mode in the present manuscript (displayed in Figure 3c). This wave has a period of about 5.25 seconds. Note, we also simulated an $n = 3$ mode and found that the results are qualitatively similar to the $n = 5$ mode results presented here. The superposition of multiple modes, as seems likely for the observed broad wave spectra, will eliminate some of the phase specific features we describe here. However, it is usually the case that the largest fluxes of field-aligned electrons of the kind presented above are observed in discrete, large amplitude intermittent features that may be described as a single mode. Our simulations specifically concern these observations.

Figure 4a displays profiles of the parallel current that results from this initial perturbation after the wave has evolved for 1.25 seconds (time of peak parallel current profile along the field line). Only the northern hemisphere of the simulation domain is shown (where $l_{||} = 0$ is the equator). The increase in the magnitude of the current as the northern low-altitude boundary is approached is due to the magnetic field convergence. However,

our primary attention is further up the field line (marked with dashed lines) where we compare the model results with Cluster and Van Allen probe observations. Figures 4c-4g show the corresponding electron distribution functions at these indicated values of $l_{||}$. The initial Maxwellian electron distribution function is plotted in Figure 4b for comparison. The $l_{||}$ values in Figures 4c-4e were chosen to capture the positions of the parallel current nodes and minimum. The values $l_{||} = 2$ and $l_{||} = 3.5\ R_E$ are approximately the positions of the the Van Allen probes and Cluster spacecraft at the times evident in Figures 1 and 2 respectively. We however, are not making a quantitative comparison between the simulations and spacecraft data at these specific locations because the field-line harmonic required for such a comparison cannot be determined from the observations. Rather, our discussion is framed more generally in terms of the qualitative spatial and temporal nature of both the simulation and observational results.

In order to understand the structure of the distribution functions at the different points along the field line it is necessary to look at the profile of the effective parallel wave potential $\Phi = -\int E_{||} dl_{||}$ (Figure 4h). We start this analysis with the field-aligned "cigar-shaped" distribution, (roughly symmetric about $v_{||} = 0$) evident in Figure 4e as it bears the closest correspondence to those evident in the Van Allen Probes observations (Figure 1). Comparison of Figures 4e and 4h indicates that the formation of this symmetric plateau corresponds to the bottom of a potential well. This situation is consistent in form with the trapped electron distribution evident in the traveling kinetic Alfvén waves considered in *Damiano et al.* [2016]. In that case, the width of the trapped electron region was shown to be consistent with the classical trapping width ($v_{tr} = \sqrt{2e\Phi/m_e}$). Repeating

that analysis here (using $|e\Phi| = 720$ eV at the bottom of the potential well in Figure 4h), the trapping width is calculated to be $\pm 1.6 \times 10^7 m/s$ (indicated by solid black parallel horizontal lines in Figure 4e) which is consistent with the parallel extent of the plateau. Initially, only colder electrons with $v_{||} \sim v_{ph}$ (close to the core of the distribution) are trapped, followed by progressively warmer ones as the wave potential grows. Trapping of this form can only occur when $-e\Phi < 0$ [e.g. *Artemyev et al.*, 2017], which explains why no trapping is evident at the current node at $l_{||} = 0$. Additionally, although we are only showing the northern hemisphere of the simulation domain, there is a symmetric trapping region at $l_{||} = -1.37\ R_E$. The equatorial region about $l_{||} = 0$ acts as a source for the trapped electrons, which appears to result in the flattening in the distributions at intermediate parallel velocities evident in Figure 4c. Low energy electrons do not have time to reach the potential wells, while high energy electrons remain un-trapped, leaving a dearth of electrons at these intermediate parallel velocities. These flattened regions are a transient feature that are manifested primarily during the growing phase of the potential wells and are then filled with the decline in well depth.

Around the node in $j_{||}$ at $l_{||} = 1.37\ R_E$ (Figure 4a), the distributions (Figures 4d and 4f) display a plateau as well, but with preferential maxima (the core of the distribution is angled) in the direction opposite in sign to that of the parallel current (compare with Figure 4a). This trend in sign between the net electron drift and the parallel current is a feature consistent with what is evident in the Cluster observations displayed in Figure 2 and it suggests that this asymmetry in the electron phase space density about $v_{||} = 0$ is how the parallel current in the wave is being carried (i.e. $j_{||} = -nev_{||}$). The period of the

resonance observed in the Cluster data is $\sim$ 14 seconds and so the long cadence time of the Van Allen Probes electron instruments (which have a nearly three time lower temporal cadence than do the particle detectors on the Cluster spacecraft) implies that the temporal features observed by Cluster would be averaged out in the Van Allen probes observations. To confirm this point, the simulated distributions were averaged over integration time scales on the order of the particle detectors on Van Allen probes. The resulting time-averaged distributions (whether at node or antinode) exhibited a symmetric plateau more consistent with what is seen in these data.

The presence of electron trapping is further supported when the evolution of electrons in the plateau regions evident in Figures 4d - 4f is examined. In Figure 4i, we followed the evolution of a subset of trapped electrons ($|v| < 2.5 \times 10^6$ m/s) close to the origin of the distribution at $l_{||} = 2\ R_E$ (Figure 4f) and, as expected, the particles stayed confined around the position of the current node for the duration of the simulation. This behavior is different than the case of the traveling wave, where the trapped electrons can be moved along the field line by the traveling mode [e.g. *Watt and Rankin*, 2009; *Artemyev et al.*, 2015; *Damiano et al.*, 2016]. As with the traveling wave case though, the period of oscillation of the particle in the potential well (τ) is inversely proportional to the magnitude of the potential $\tau \propto 1/\sqrt{\Phi}$ [e.g. *Damiano et al.*, 2016]. Since the magnitude of the parallel electric field is directly proportional to the electron temperature [e.g. *Hasegawa and Chen*, 1976; *Lysak and Lotko*, 1996; *Cheng and Johnson*, 1999; *Chaston et al.*, 2003], τ becomes shorter as the electron temperature is increased. This trapping is not permanent though. As the potential grows and declines over an Alfvén cycle, electrons can become

trapped and then de-trapped, but since the primary purpose of this letter is a qualitative comparison between the simulation and observations, a more detailed analysis of this long term evolution will be left to a follow-up manuscript.

While the simulations do reproduce the qualitative features of the observations quite well, the cigar-shaped plateau is less well represented in the simulations than in the Cluster observations. This difference is most likely associated with the lack of a cold plasma population in the model. The Cluster observations on the other hand illustrate that the distributions are composed of two components: a hot plasma sheet component and a cold component of ionospheric origin. This cold component increases the availability of electrons at low energies to be trapped in the wave potential, enhancing the elongated core feature's evident in Figure 2 relative to the simulation generated distribution functions evident in Figure 4. We will consider a second cold electron population in the simulations in a future study.

Another interesting point of comparison are the prominent loss cone features that appear at 180^o pitch angle in both the simulations (Figures 4f and 4g) and Cluster observations (Figures 2g and 2i) and to a lesser extent in the Van Allen probes data as well (Figure 1d). *Hull et al.* [2016] attributes the loss cone features in the Cluster data to potential drops below the spacecraft due to upward directed parallel electric fields which act to prevent ionospheric photoelectrons or backscattered electrons from reaching the spacecraft altitudes. The resulting situation is similar in the simulations. Electrons not trapped by the potential well centered at $l_{||} = 1.37\ R_E$, and sourced primarily between the potential well and the ionosphere, are accelerated downward by upward directed parallel electric

fields at altitudes below the potential well. Accelerated electrons reaching the field-aligned boundary of the model are then precipitated out of the simulation domain. Although the model lacks an ionospheric electron population or backscattered electrons, the presence of the downward accelerating parallel electric fields, that in reality inhibit the propagation of these up-going electrons, allows the simulation to reproduce the Cluster observations reasonably well. Additionally, although the potential well acts primarily to trap electrons, higher energy electrons sourced from within this region also contribute to the electron precipitation as illustrated by the loss cone features evident in Figures 4d to 4f. These features are less well defined than in Figure 4g because the large parallel extent of the trapping width pushes the velocity space affected by the precipitation of un-trapped electrons to higher parallel energies (that are poorly sampled in the simulation distribution of electrons). The prominence of the loss cone features also becomes progressively reduced as the equatorial region is approached. This trend is consistent with the slight loss cone feature evident in the Van Allen Probes observations (Figure 1d) which is closer to the equatorial plane.

Finally, it should be noted that there are several possible explanations for the loss cone features seen in the observations, including quasi-static potential drops and double layers (Alfvén related or not). However, the consistency between the simulation results and the Cluster observations suggest that wave potentials associated with KFLRs are another candidate.

4. Conclusions

In this work, we have studied the electron dynamics within a kinetic scale field line resonance (KFLRs) and compared the simulated electron distributions with that seen in Cluster and Van Allen probes observations. These comparisons provide a qualitative confirmation of the action of electron trapping in the potential associated with the observed wave fields as well as the action of the potential on untrapped high energy electrons.

Both the simulations and observations show a plateaued elongated form and counter-streaming along $v_{||}$ over an energy range that is consistent with the expected trapping in the wave potential. Depending on location along the field-line, and/or wave phase, peaks in phase space density can be identified in the simulations and observations in both the downgoing and upgoing directions consistent with the sign of the field-aligned current. At higher energies, both the simulations and observations illustrate loss cones features in the field opposed direction due to the action of the wave parallel electric field on the un-trapped electron populations. The agreement between these features supports the veracity of the modeling while providing a self-consistent description for electron trapping, precipitation and current closure within KFLRs.

These quantitative comparisons between the observed and simulated distributions are compromised by the presence of a cold electron component at Cluster, the unknown harmonic composition of the observed wave-fields and temporal aliasing in the Van Allen Probe electron measurements. The first is responsible for the highly field-aligned component in the core of the distributions measured from Cluster and not well represented in the simulation results. The second leads to ambiguity in relating the observed distributions

to the eigenmode structure of the simulation. The third averages the electron distribution over a large fraction of a wave period to smooth out physical asymmetries at the Van Allen Probes associated with wave phase.

Acknowledgments. P. Damiano acknowledges useful discussions with E.A. Startsev on particle trapping in standing waves. The authors acknowledge support from NASA grant NNH16AC43I and NSF grant AGS1203299. J. Johnson was additionally supported by NASA grant NNX16AR10G and NSF grant AGS1405225. P. Damiano was also supported by NASA grant NNH14AY20I and NSF grant AGS1602972. C. Chaston acknowledges support from NASA grant NNX15AF57G and NSF Grant AGS1602941. Support for A.J. Hull was also provided by NASA grant NNX12AD24G. Computing resources were provided by the Princeton Plasma Physics Laboratory, the Geophysical Institute at the University of Alaska Fairbanks and the National Center for Atmospheric Research (under CISL project UPR10002). Numerical simulation data used in the figures is stored at the Geophysical Institute and may be accessed by contacting the corresponding author (padamiano@alaska.edu). Van Allen Probes measurements used in this study can be obtained from the following data repositories: EFW http://www.space.umn.edu/rbspefw-data/, HOPE/MAGEIS/REPT https://www.rbsp-ect.lanl.gov/science/DataDirectories.php, and/or by directly contacting C. Chaston (cchaston@berkeley.edu). Cluster observations used in this study are available at https://www.cosmos.esa.int/web/csa and/or by contacting A. Hull (ahull@berkeley.edu).

References

Artemyev, A. V., R. Rankin, and M. Blanco (2015), Electron trapping and acceleration by kinetic Alfvén waves in the inner magnetosphere, *Journal of Geophysical Research (Space Physics)*, *120*, 10, doi:10.1002/2015JA021781.

Artemyev, A. V., R. Rankin, and I. Y. Vasko (2017), Nonlinear Landau resonance with localized wave pulses, *Journal of Geophysical Research (Space Physics)*, *122*, 5519–5527, doi:10.1002/2017JA024081.

Chaston, C. C., C. W. Carlson, W. J. Peria, R. E. Ergun, and J. P. McFadden (1999), FAST Observations of Inertial Alfvén Waves in the Dayside Aurora, *Geophys. Res. Lett.*, *26*, 647–650, doi:10.1029/1998GL900246.

Chaston, C. C., J. W. Bonnell, C. W. Carlson, J. P. McFadden, R. J. Strangeway, and R. E. Ergun (2003), Kinetic effects in the acceleration of auroral electrons in small scale Alfvén waves: A FAST case study, *Geophys. Res. Lett.*, *30*, 1289, doi:10.1029/2002GL015777.

Chaston, C. C., J. W. Bonnell, J. R. Wygant, C. A. Kletzing, G. D. Reeves, A. Gerrard, L. Lanzerotti, and C. W. Smith (2015), Extreme ionospheric ion energization and electron heating in Alfvén waves in the storm time inner magnetosphere, *Geophys. Res. Lett.*, *42*, doi:10.1002/2015GL066674.

Chaston, C. C., J. W. Bonnell, J. R. Wygant, G. D. Reeves, D. N. Baker, D. B. Melrose, and I. H. Cairns (2017), Radial transport of radiation belt electrons in kinetic field-line resonances, *Geophys. Res. Lett.*, *44*, 8140–8148, doi:10.1002/2017GL074587.

Chaston, C. C., et al. (2014), Observations of kinetic scale field line resonances, *Geophys. Res. Lett.*, *41*, 209–215, doi:10.1002/2013GL058507.

Cheng, C. Z., and J. R. Johnson (1999), A kinetic-fluid model, *J. Geophys..Res.*, *104*, 413–428, doi:10.1029/1998JA900065.

Claudepierre, S. G., M. K. Hudson, W. Lotko, J. G. Lyon, and R. E. Denton (2010), Solar wind driving of magnetospheric ULF waves: Field line resonances driven by dynamic pressure fluctuations, *Journal of Geophysical Research (Space Physics)*, *115*, A11202, doi:10.1029/2010JA015399.

Claudepierre, S. G., F. R. Toffoletto, and M. Wiltberger (2016), Global MHD modeling of resonant ULF waves: Simulations with and without a plasmasphere, *Journal of Geophysical Research (Space Physics)*, *121*, 227–244, doi:10.1002/2015JA022048.

Damiano, P. A., and J. R. Johnson (2012), Electron acceleration in a geomagnetic Field Line Resonance, *Geophys. Res. Lett.*, *39*, L02102, doi:10.1029/2011GL050264.

Damiano, P. A., and A. N. Wright (2008), Electron thermal effects in standing shear Alfvén waves, *Journal of Geophysical Research (Space Physics)*, *113*, A09219, doi: 10.1029/2008JA013087.

Damiano, P. A., R. D. Sydora, and J. C. Samson (2003), Hybrid magnetohydrodynamic-kinetic model of standing shear Alfvén waves, *Journal of Plasma Physics*, *69*, 277–304, doi:10.1017/S0022377803002216.

Damiano, P. A., A. N. Wright, R. D. Sydora, and J. C. Samson (2005), Hybrid magentohydrodynamic-kinetic electron closure methods and shear Alfvén waves in nonuniform plasmas, *Phys. Plasmas*, *12*, 042,105.

Damiano, P. A., A. N. Wright, R. D. Sydora, and J. C. Samson (2007), Energy dissipation via electron energization in standing shear Alfvén waves, *Phys. Plasmas*, *14*, 062,904.

Damiano, P. A., J. R. Johnson, and C. C. Chaston (2015), Ion temperature effects on magnetotail Alfvén wave propagation and electron energization, *Journal of Geophysical Research (Space Physics)*, *120*, 5623–5632, doi:10.1002/2015JA021074.

Damiano, P. A., J. R. Johnson, and C. C. Chaston (2016), Ion gyroradius effects on particle trapping in kinetic Alfvén waves along auroral field lines, *Journal of Geophysical Research (Space Physics)*, *121*, 10, doi:10.1002/2016JA022566.

Denton, M. H., M. F. Thomsen, H. Korth, S. Lynch, J. C. Zhang, and M. W. Liemohn (2005), Bulk plasma properties at geosynchronous orbit, *Journal of Geophysical Research (Space Physics)*, *110*, A07223, doi:10.1029/2004JA010861.

Elkington, S. R. (2006), A Review of ULF Interactions With Radiation Belt Electrons, in *Magnetospheric ULF Waves: Synthesis and New Directions*, *Washington DC American Geophysical Union Geophysical Monograph Series*, vol. 169, edited by K. Takahashi, P. J. Chi, R. E. Denton, and R. L. Lysak, p. 177, doi:10.1029/169GM12.

Hasegawa, A., and L. Chen (1976), Kinetic processes in plasma heating by resonant mode conversion of Alfvén wave], *Physics of Fluids*, *19*, 1924–1934, doi:10.1063/1.861427.

Hudson, M. K., B. T. Kress, H.-R. Mueller, J. A. Zastrow, and J. Bernard Blake (2008), Relationship of the Van Allen radiation belts to solar wind drivers, *Journal of Atmospheric and Solar-Terrestrial Physics*, *70*, 708–729, doi:10.1016/j.jastp.2007.11.003.

Hull, A. J., C. C. Chaston, H. U. Frey, M. O. Fillingim, M. L. Goldstein, J. W. Bonnell, and F. S. Mozer (2016), The "Alfvénic surge" at substorm onset/expansion and the formation of "Inverted Vs": Cluster and IMAGE observations, *Journal of Geophysical Research (Space Physics)*, *121*, 3978–4004, doi:10.1002/2015JA022000.

Li, Z., M. Hudson, J. Paral, M. Wiltberger, and D. Turner (2016), Global ULF wave analysis of radial diffusion coefficients using a global MHD model for the 17 March 2015 storm, *Journal of Geophysical Research (Space Physics)*, *121*, 6196–6206, doi: 10.1002/2016JA022508.

Lotko, W., A. V. Streltsov, and C. W. Carlson (1998), Discrete auroral arc, electrostatic shock and suprathermal electrons powered by dispersive, anonamously resistive field line resonance, *Geophys. Res. Lett.*, *25*, 4449.

Lysak, R. L., and W. Lotko (1996), On the kinetic dispersion relation for shear Alfvén waves, *J. Geophys. Res.*, *101*, 5085–5094, doi:10.1029/95JA03712.

Nakamura, T. K. (2000), Parallel electric field of a mirror kinetic Alfvén wave, *J. Geophys. Res.*, *105*, 10,729–10,738, doi:10.1029/1999JA900494.

Rankin, R., J. C. Samson, and P. Frycz (1993), Simulations of driven field line resonances in the Earth's magnetosphere, *J. Geophys. Res.*, *98*, 21, doi:10.1029/93JA02083.

Rankin, R., P. Frycz, V. T. Tikhonchuk, and J. C. Samson (1994), Nonlinear standing shear Alfvén waves in the Earth's magnetosphere, *J. Geophys. Res.*, *99*, 21,291–21,302, doi:10.1029/94JA01629.

Rankin, R., C. E. J. Watt, and J. C. Samson (2007), Self-consistent wave-particle interactions in dispersive scale long-period field-line-resonances, *Geophys.Res. Lett.*, *34*, L23103, doi:10.1029/2007GL031317.

Rickard, G. J., and A. N. Wright (1994), Alfvén resonance excitation and fast wave propagation in magnetospheric waveguides, *J. Geophys. Res.*, *99*, 13,455, doi: 10.1029/94JA00674.

Samson, J. C., R. Rankin, and V. T. Tikhonchuk (2003), Optical signatures of auroral arcs produced by field line resonances: Comparison with satellite observations and modeling, *Ann. Geophys.*, *21*, 933.

Streltsov, A., and W. Lotko (1995), Dispersive field line resonances on auroral field lines, *Journal of Geophysical Research*, *100*, 19,457–19,472, doi:10.1029/95JA01553.

Streltsov, A. V., and W. Lotko (1997), Dispersive, nonradiative field line resonances in a dipolar magnetic field geometry, *J. Geophys. Res.*, *102*, 27,121–27,136, doi: 10.1029/97JA02530.

Streltsov, A. V., W. Lotko, J. R. Johnson, and C. Z. Cheng (1998), Small-scale, dispersive field line resonances in the hot magnetospheric plasma, *J. Geophys. Res.*, *103*, 26,559–26,572, doi:10.1029/98JA02679.

Taylor, J. P. H., and A. D. M. Walker (1984), Accurate approximate formulae for toroidal standing hydromagnetic oscillations in a dipolar geomagnetic field, *Planet. Space Sci.*, *32*, 1119–1124, doi:10.1016/0032-0633(84)90138-7.

Voronkov, I., R. Rankin, V. T. Tikhonchuk, and J. C. Samson (1997), Nonlinear shear Alfvén resonances in a dipolar magnetic field, *J. Geophys. Res.*, *102*, 27,137–27,144, doi:10.1029/97JA02533.

Watt, C. E. J., and R. Rankin (2009), Electron Trapping in Shear Alfvén Waves that Power the Aurora, *Physical Review Letters*, *102*(4), 045002, doi: 10.1103/PhysRevLett.102.045002.

Wei, C. Q., J. C. Samson, R. Rankin, and P. Frycz (1994), Electron inertial effects on geomagnetic field line resonances, *J. Geophys. Res.*, *99*, 11,265–11,276, doi:

10.1029/94JA00582.

Wygant, J. R., et al. (2002), Evidence for kinetic Alfvén waves and parallel electron energization at 4-6 R_E altitudes in the plasma sheet boundary layer, *Journal of Geophysical Research (Space Physics)*, *107*, 1201–+, doi:10.1029/2001JA900113.

Xu, B. L., J. C. Samson, W. W. Liu, F. Creutzberg, and T. J. Hughes (1993), Observations of optical aurora modulated by resonant Alfvén waves, *J. Geophys. Res.*, *98*, 11,531.

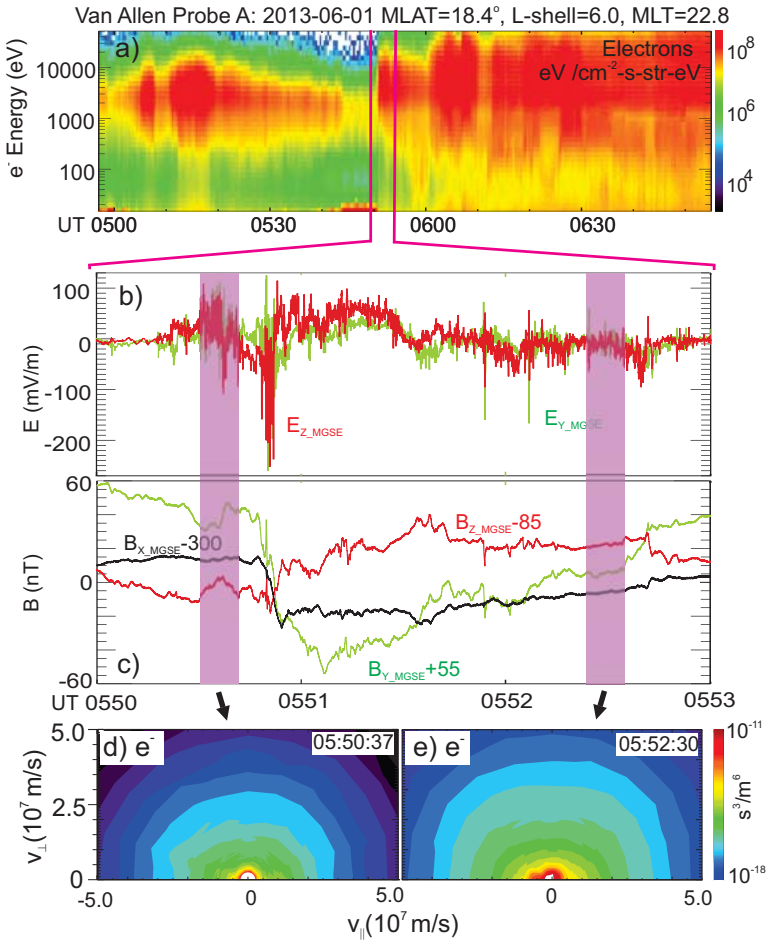

Figure 1. Kinetic Alfvénic fluctuations and parallel electron heating. a) Geomagnetic storm-time electron spectrogram; b) and c) zoom-in on electromagnetic field variations in a spacecraft coordinate system close to GSE coordinates; d) and e) electron distribution snapshots captured during the interval shown in preceding panels showing evidence for geomagnetic field-aligned acceleration/heating (Figure modified from *Chaston et al.* [2015]).

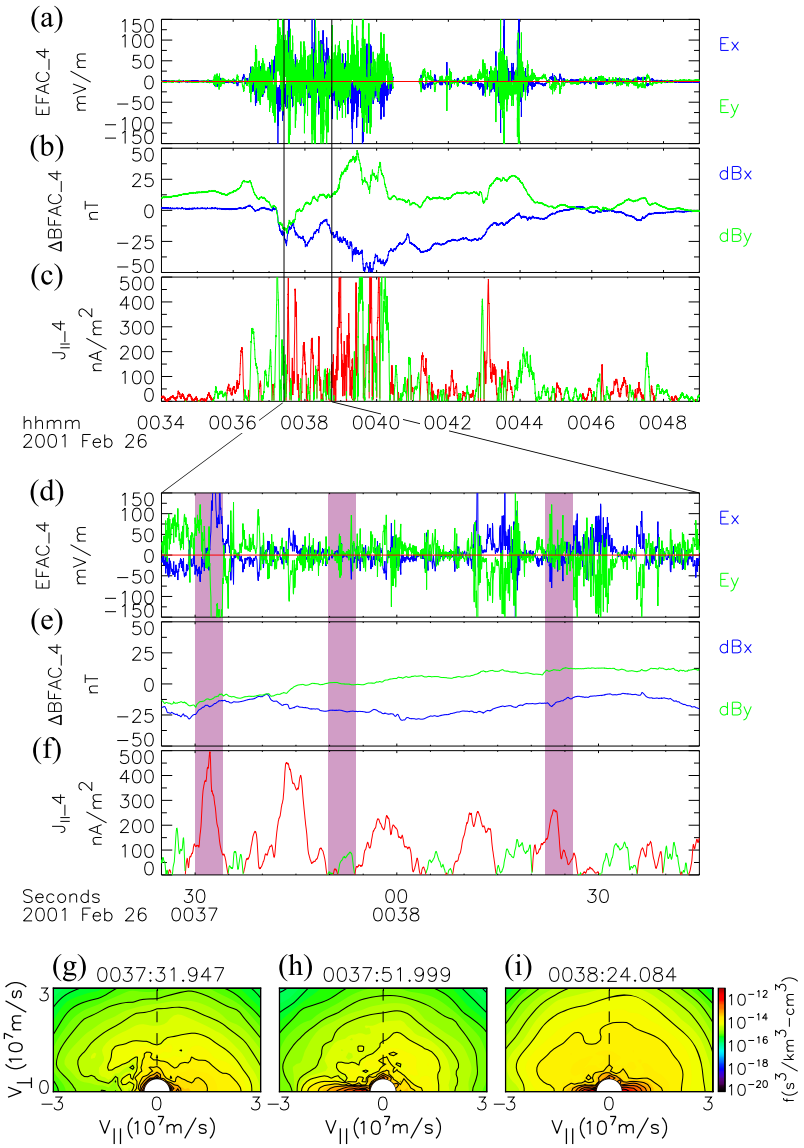

Figure 2. (a) Electric and (b) perturbation magnetic fields as observed by the Cluster 4 spacecraft in a field aligned coordinate (where only perpendicular components are shown) along with the (c) magnitude of the parallel current. For parallel current, red and green lines indicate upward and downward current, respectively. (d)-(f) Zoom in of top panels for selected time interval. (g)-(i) Electron distribution functions at the times indicated by the solid vertical lines in (d)-(f). Distributions compiled using PEACE-HEEA detector on the Cluster 4 spacecraft which samples electron counts from 30 eV to 26 keV.

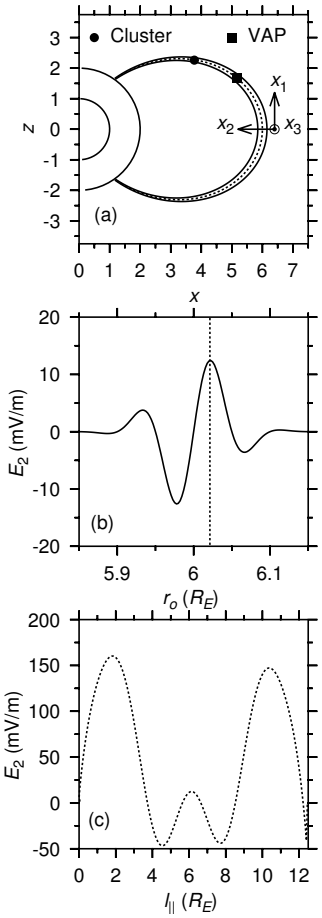

Figure 3. a): Simulation domain where x_3 is positive increasing out of the page. Solid lines denote the $L = 5.85$ and $L = 6.15$ perpendicular boundary field lines. The dotted line indicates the $L = 6$ field line (along which the maximum parallel current of the wave perturbation occurs). The circles of radius 1 and 2 R_E respectively denote the surface of the Earth and low altitude "ionospheric" boundary, while the filled square and circle denote the approximate positions of the Van Allen Probes (VAP) and Cluster 4 spacecraft in Figures 1 and 2 respectively . b) Initial radial (E_2) electric field profile as a function of r_o ($r = r_o \sin^2\theta$, where the angle θ is subtended from the z axis) at the equator. (c) E_2 as a function of field line length $l_{||}$ (measured from the southern low-altitude boundary). Profile taken along dotted line plotted in Figure 3b.

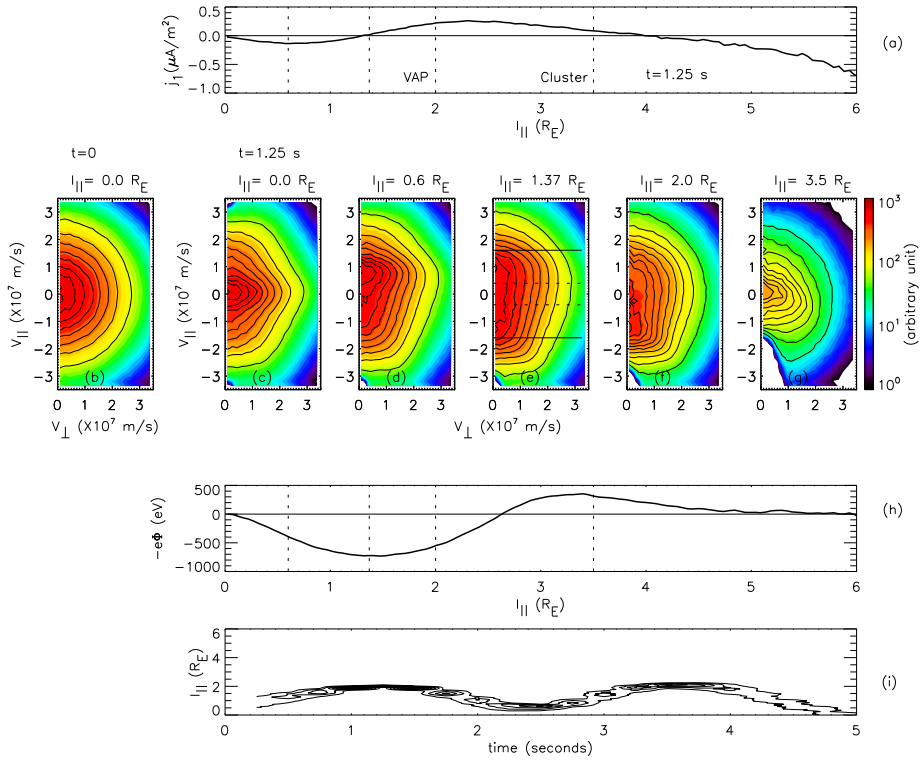

Figure 4. a) Parallel current density as a function of distance along the field line ($l_{||}$ - measured from equator) at $t = 1.25$ s. (b) Initial Maxwellian distribution function at $t = 0$. (c)-(g) Electron distribution functions at $t = 1.25$ s and the indicated values of $l_{||}$ (also identified by the vertical dashed lines in panels (a) and (h)). Parallel dashed lines in Figure 4e illustrate phase velocity ($\pm v_{ph}$) of wave (assuming $k_\perp \rho_i \sim 1$ so that $v_{ph} = \omega/k_{||} \sim \sqrt{2}V_A$) while the parallel solid lines indicate the theoretical trapping width $\pm v_{tr}$. (h) Effective potential ($\Phi = -\int E_{||} dl_{||}$) at $t = 1.25$ s. Note: In Figures 4c-h, $v_\perp = \sqrt{v_2^2 + v_3^2}$ is the gyro-averaged perpendicular velocity and $v_{||} = v_1$. (i) Evolution of an ensemble of trapped electrons taken from core of distribution evident in Figure 4f. The internal structure is associated with the interval at which particle data was saved in the simulation run.